IOP Publishing Physica Scripta
Phys. Scr. 95 (2020) 045401 (8pp) https://doi.org/10.1088/1402-4896/ab5e8f

# Positron-impact single ionization of helium using the Faddeev–Merkuriev equations

**M Silenou Mengoue, D E Bokwa Ngombo and Arnaud Denabe**

Centre for Atomic, Molecular Physics and Quantum Optics, Faculty of Science, University of Douala, PO Box 8580, Douala, Cameroon

E-mail: smengoue@yahoo.fr

Received 21 October 2019, revised 29 November 2019
Accepted for publication 4 December 2019
Published 12 February 2020

**Abstract**

We present the study of the positron-impact single ionization process of helium in the case where the residual ion remains in its ground state. We calculated the total cross-section for incident-positron energies ranging from the ionization threshold to 150 eV, and the triple differential cross-sections (TDCSs), using a single continuum wave function built through the Faddeev–Merkuriev differential equations. A comparison of the results of the total cross-section obtained with our approach and other theoretical models as well as with existing experimental data, shows a good agreement. Due to the lack of experimental and theoretical results for comparison, and to be more general and predictable in our investigation, the two- and three-dimensional representation of the TDCSs covering all possible values of the angle of the ejected electron for different values of its energy are presented and discussed.

Keywords: Faddeev–Merkuriev equations, positron-atom scattering, total and triple differential cross-sections

(Some figures may appear in colour only in the online journal)

## 1. Introduction

The single ionization of atoms and molecules is one of the most important areas of collision physics. More particularly, positron scattering is fundamentally important for the understanding of the structure of matter and the dynamics of the collisional process. It presents also a special interest for the use of the positron emission tomography scanner to make diagnosis of cancer in medicine and the positron annihilation lifetime spectroscopy, to analyse and design specific materials in material science [1–3].

The first calculations of $e^+ - \mathrm{He}$ scattering have been performed by Massey and Moussa [4] in the first born approximation (FBA). From the FBA studies, more sophisticated and significant theoretical advances have been made for describing the dynamic of the ionization of helium by positronic impact and there is now good agreement between experimental and theoretical results for this atom, especially while talking about total cross-sections. The distorted-wave Born approximation (DWBA) was applied by Parcell *et al* [5] using the distorted wavefunctions in first-order calculations, and later by Campeanu *et al* [6] using Coulomb and plane wavefunctions. The second group obtained accurate results in agreement with the experimental results of Knudsen *et al* [7] and Moxom *et al* [8]. The Kohn variational method was applied by Humberston *et al* [9] and by Van-Reeth and Humberston [10]. There is a very good agreement for the total cross section below the Ps-formation (Positronium-formation) threshold between their results and the experimental data of Mizogawa *et al* [11] and Stein *et al* [12]. Many other methods have been used in order to approximate the exact solution of the scattering problem in $e^+ -$ He systems; such as the close-coupling approach by Campbell *et al* [13], the hyper-spherical close-coupling approach by Igarashi *et al* [14], the frozen-core and multi-core convergent close-coupling [15–17] and the works of the UCL group [18–20]. Recently, total and integral cross sections from the application of optical potential model to positron scattering from gas-phase beryllium and magnesium have been reported [21]. Despite the enormous progress made so far in discretization and subsequent numerical solutions of three-body differential and integral equations of the Coulomb scattering theory, a number of related problems remain open.

In this contribution, in addition to the total cross-section, we are interested by the triple differential cross-sections

 

(TDCSs) of a positron-impact single ionization of helium. Some earlier theoretical studies of the TDCSs for positron scattering may be found in [22–24], but these calculations were restricted to atomic hydrogen. Besides these studies, some experimental works for positron impact ionization of some inert gases have been made [25–27] but not for helium. *Overall, there is a lack of studies devoted to TDCSs of* a positron-impact single ionization of helium. *The present contribution aims to partially fill this gap.*

In this paper, we use a compact-kernel-integral-equation approach built from the Faddeev–Merkuriev differential equations [28, 29] to calculate a three-body wave function that describes the single continuum of an atomic two-electron system. We then applied it to positron-impact single ionization of helium. Here, the residual ion remains in its ground state and we are limited in this work to the treatment of the channel of single ionization without taking the positronium formation and other channels into account. The calculation is performed for asymmetric coplanar geometry. The result for the total positron–helium scattering cross section is firstly presented for incident-positron energies ranging from the ionization threshold to 150 eV. To be more general and predictable in our investigation, the two- and three-dimensional representation of the TDCS's covering all possible values of the angle of the ejected electron for different values of its energy are presented. The energy of the incident positron for the latter case is fixed at 700 eV.

The paper is organized as follows. After this introduction, in the second section, we briefly present the theoretical approach used. The third section is devoted to the results and discussion. Firstly, the plots of the short and long range potentials used in Faddeev decomposition are shown; follow by a representation of the Merkuriev cut-off function used. Secondly, the result for the total positron–helium scattering cross section is presented and compare to existing theoretical and experimental data. Thirdly, the two- and three-dimensional representation of the TDCS's are presented and discussed. The paper ends in section four with a brief summary. Atomic units are used throughout.

## 2. Theory

The Hamiltonian of a three-body atomic system is given by:

$$H = \sum_{i=1}^{2}\left(-\frac{1}{2}\Delta_i - \frac{Z}{r_i}\right) + \frac{1}{r_{12}}, \tag{1}$$

where $\mathbf{r}_i$ are the position vectors of the two electrons. $r_{12} = |\mathbf{r}_2 - \mathbf{r}_1|$ is the interelectronic distance. $Z = 2$ denotes the charge of the infinitely massive nucleus the position of which coincides with the origin of the laboratory system. The continuum wave function with an asymptotic ingoing wave behavior is a solution of the following Schrödinger equation:

$$(H - E)\Psi^{(-)}(\mathbf{r}_1, \mathbf{r}_2) = 0, \tag{2}$$

where $E$ is the total energy of the two electrons. Following Faddeev and Merkuriev [30], we split the electron-nucleus Coulomb potentials into a short and a long range part:

$$\frac{Z}{r_i} = V_i^{(s)}(r_1, r_2) + V_i^{(l)}(r_1, r_2), \tag{3}$$

where

$$V_i^{(s)}(r_1, r_2) = \frac{Z}{r_i}\,\zeta(r_i, r_j),$$
$$V_i^{(l)}(r_1, r_2) = \frac{Z}{r_i}[1 - \zeta(r_i, r_j)], \tag{4}$$

and

$$\zeta(r_i, r_j) = 2/\{1 + \exp[(r_i/a)^{\nu}/(1 + r_j/b)]\}. \tag{5}$$

The subscripts $i$ and $j$ take the value 1 or 2 with $i \neq j$. The role of $\zeta(r_i, r_j)$ is to fix a border between $\Omega_0$, the so-called 'true' three-body scattering region (where $r_1 \sim r_2$), and the two-body scattering regions $\Omega_1$ ($r_1 \gg r_2$), or $\Omega_2$ ($r_2 \gg r_1$)

$$\lim_{r_2, r_1 \to \infty} \zeta(r_2, r_1) \longrightarrow \begin{cases} 1 & \text{in } \Omega_2(r_2 > r_1^{\nu}),\ \nu > 2; \\ 0 & \text{otherwise.} \end{cases} \tag{6}$$

The representation of the long and short range potentials is shown on figure 1. A representation of the cut-off function used is also presented on figure 2.

Both electrons are identical particles, so we can introduce the new functions $\Psi_i^{(-)}(\mathbf{r}_1, \mathbf{r}_2)$ ($i = 1, 2$), such that $\Psi^{(-)} = (1/\sqrt{2})[\Psi_1^{(-)} + \Psi_2^{(-)}]$. Taking into account the exchange symmetry of the solution of equation (2), $\Psi^{(-)}(\mathbf{r}_1, \mathbf{r}_2) = \epsilon\,\Psi^{(-)}(\mathbf{r}_2, \mathbf{r}_1)$, where $\epsilon = +1$ $(-1)$ for a singlet (triplet) state, we have: $\Psi_2^{(-)}(\mathbf{r}_1, \mathbf{r}_2) = \epsilon\,\hat{P}_{12}\Psi_1^{(-)}(\mathbf{r}_1, \mathbf{r}_2)$, where $\hat{P}_{12}$ is the permutation operator of particle indices 1 and 2. Thus

$$\Psi^{(-)} = (1/\sqrt{2})[1 + \epsilon\hat{P}_{12}]\Psi_1^{(-)}. \tag{7}$$

Now we demand that the functions $\Psi_1^{(-)}$ and $\Psi_2^{(-)}$ satisfy the following equations of Faddeev type:

$$\left[E + \frac{1}{2}\,\Delta_1 + \frac{1}{2}\,\Delta_2 + V_1^{(l)} + V_2^{(l)} - \frac{1}{r_{12}}\right] \times \Psi_1^{(-)} = -\sqrt{2}\,V_2^{(s)}\Psi^{(-)}, \tag{8}$$

$$\left[E + \frac{1}{2}\,\Delta_1 + \frac{1}{2}\,\Delta_2 + V_1^{(l)} + V_2^{(l)} - \frac{1}{r_{12}}\right] \times \Psi_2^{(-)} = -\sqrt{2}\,V_1^{(s)}\Psi^{(-)}. \tag{9}$$

According to the previous discussion, and using equation (7) we can rewrite equation (8) as:

$$\left[E + \frac{1}{2}\,\Delta_1 + \frac{1}{2}\,\Delta_2 + V_1^{(l)} + V_2^{(l)} - \frac{1}{r_{12}}\right] \times \Psi_1^{(-)} = -V_2^{(s)}(1 + g\hat{P}_{12})\Psi_1^{(-)}. \tag{10}$$

Equation (9) can be transformed in exactly the same way. As a results, we obtain only one equation for the component $\Psi_1^{(-)}(\mathbf{r}_1, \mathbf{r}_2)$, which is fully equivalent to equation (2). Let us now rewrite equation (10) in the following way:

$$\left[E + \frac{1}{2}\,\Delta_1 + \frac{1}{2}\,\Delta_2 + \frac{Z-1}{r_1} + \frac{Z}{r_2}\right]\Psi_1^{(-)} = V(\mathbf{r}_1, \mathbf{r}_2)\Psi_1^{(-)}, \tag{11}$$

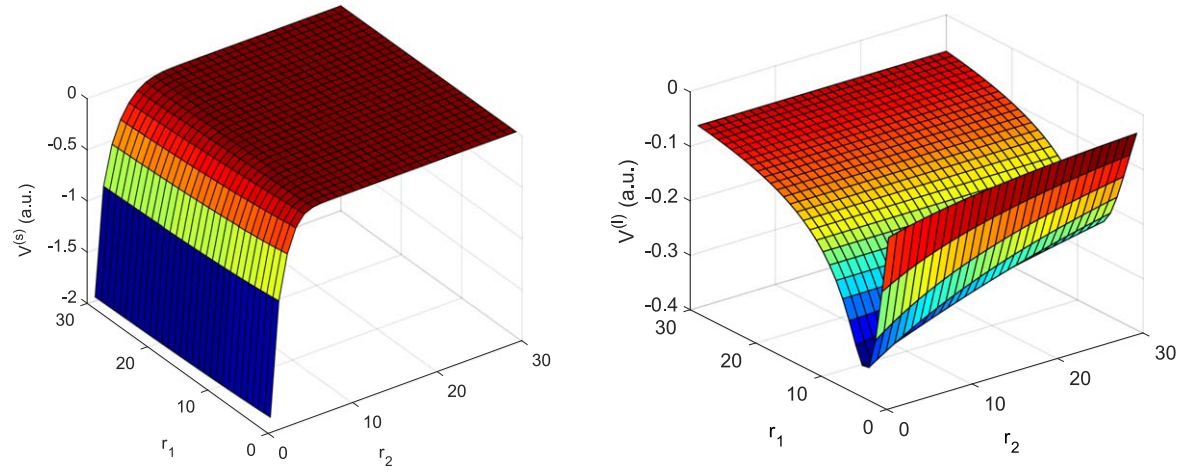


**Figure 1.** The short-range $V^{(s)}$ and long-range $V^{(l)}$ potentials.

where:

$$V(\mathbf{r}_1, \mathbf{r}_2) = -V_1^{(l)}(r_1, r_2) + \frac{Z-1}{r_1} - gV_2^{(s)}(r_1, r_2)\widehat{P}_{12} + \frac{1}{r_{12}}. \tag{12}$$

It is straightforward to see that the potential $V(\mathbf{r}_1, \mathbf{r}_2)$ is short-range in the two-body scattering region $\Omega_2$ ($r_2 \gg r_1$).

We can now perform a partial wave decomposition of the wave function $\Psi_1^{(-)}$ and write:

$$\Psi_1^{(-)}(\mathbf{r}_1, \mathbf{r}_2) = \sqrt{\frac{2}{\pi}}\frac{1}{p}\sum_{L'M'}\sum_{\lambda' l' \mu'} \times \langle \lambda' \mu' m' |\, L' M' \rangle y^*_{\lambda' \mu'}(\hat{p})\psi^{L'M'}_{\lambda' l'}(\mathbf{r}_1, \mathbf{r}_2; E), \tag{13}$$

$L'$ is the total angular momentum and $M'$ its projection on the quantization axis. The Clebsch–Gordon coefficient is written according to the 3j symbols [31]:

$$\langle \lambda' \mu' l' m' |\, L' M' \rangle \equiv C \begin{matrix} M' & \lambda' & l' \\ L' & \mu' & m' \end{matrix} = \sqrt{2L'+1}(-1)^{\lambda' - l' + M'} \begin{pmatrix} \lambda' & l' & L' \\ \mu' & m' & -M' \end{pmatrix}. \tag{14}$$

In the equation (13), the spatial wave function $\psi^{L'M'}_{\lambda' l'}(\mathbf{r}_1, \mathbf{r}_2; E)$ can be further expanded in a basis of Coulomb Sturmian functions [32] and bipolar harmonics:

$$\psi^{L'M'}_{\lambda' l'}(\mathbf{r}_1, \mathbf{r}_2; E) = \sum_{\nu' n', \lambda' l'} b^{L'(\lambda' l')}_{\nu' n'}(E)\langle \mathbf{r}_1, \mathbf{r}_2 | \nu' \lambda' n' l';\ L' M' \rangle, \tag{15}$$

with

$$\langle \mathbf{r}_1, \mathbf{r}_2 | \nu' \lambda' n' l';\ L' M' \rangle = \frac{S^{\kappa}_{\nu' \lambda'}(r_1)}{r_1}\frac{S^{\kappa}_{n' l'}(r_2)}{r_2}\Lambda^{L'M'}_{\lambda' l'}(\hat{r}_1, \hat{r}_2). \tag{16}$$

$\Lambda^{L'M'}_{\lambda' l'}(\hat{r}_1, \hat{r}_2)$ is the bipolar harmonics. The Coulomb Sturmian functions $S^{\kappa}_{nl}(r)$ form a complete and discrete set of

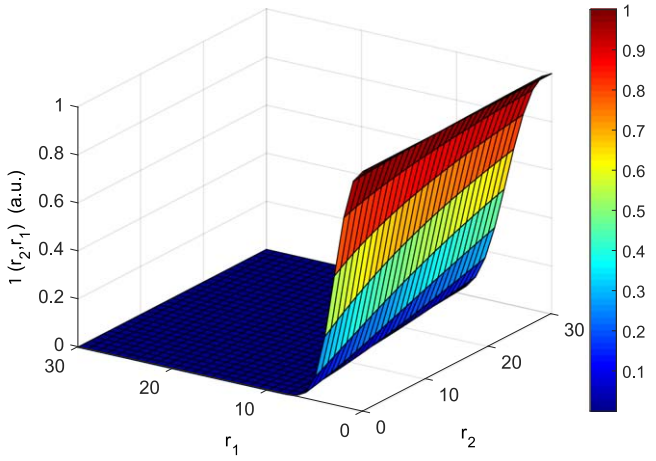


**Figure 2.** Merkuriev cut-off function with parameters $a = 3$, $b = 20$, and $\nu = 2.1$.

$\mathcal{L}^2$-integrable functions defined as follows:

$$S^{\kappa}_{nl}(r) = \left(\frac{\kappa(n-l-1)!}{n(n+l)!}\right)^{1/2} \times (2\kappa r)^{l+1}\mathrm{e}^{-\kappa r}L^{2l+1}_{n-l-1}(2\kappa r), \quad n \geqslant l+1, \tag{17}$$

where $\kappa$ is a nonlinear basis parameter. $L^{\alpha}_n(x)$ is a Laguerre polynomial [33]. These functions are known to be orthogonal with the weight $1/r$

$$\int_0^{\infty} \frac{\mathrm{d}r}{r} S^{\kappa}_{nl}(r)S^{\kappa}_{n' l}(r) = \frac{\kappa}{n}\delta_{nn'}.$$

Equation (13) taking into account equations (14)–(16) can now be written:

$$\Psi_1^{(-)}(\mathbf{r}_1, \mathbf{r}_2) = \sqrt{\frac{2}{\pi}}\frac{1}{p}\sum_{L'M'}\sum_{\lambda' l', \nu', n'} \times \sqrt{2L'+1}(-1)^{\lambda' - l' + M'}\begin{pmatrix} \lambda' & l' & L' \\ \mu' & m' & -M' \end{pmatrix} \times b^{L'(\lambda' l')}_{\nu' n'}(E) \times \frac{S_{\nu' \lambda'}}{r_1}\Lambda^{L'M'}_{\lambda' l'}(\hat{r}_1, \hat{r}_2)\frac{S_{n' l'}}{r_2}. \tag{18}$$

After some calculations [34, 35], the coefficients $b_{\nu' n'}^{L'(\lambda' l')}(E)$ are obtained in the form:

$$b_{\nu' n'}^{L'(\lambda' l')}(E) = (\mathrm{i}^{\lambda} \mathrm{e}^{-\mathrm{i}(\sigma_\lambda)} s_{\nu\lambda}(p, Z-1) s_{nl_0}^{(n_0)}) \delta_{l,l_0} + \sum_{\lambda,'l,'\nu,\nu',n,n'} G_{\nu\nu',nn'}^{\lambda l((-)}(E) V_{\nu n,\nu' n'}^{L(\lambda l)(\lambda' l')} b_{\nu' n'}^{L(\lambda' l')}(E), \tag{19}$$

where

$$V_{n\nu,n'\nu'}^{L(l\lambda)(l'\lambda')} = \langle n\ l\ \nu\ \lambda;\ LM |\ V(\mathbf{r}_1, \mathbf{r}_2) | n'\ l'\ \nu'\ \lambda';\ LM \rangle, \tag{20}$$

denotes a matrix element of the potential defined by equation (12) in the basis (17). Since in this work we are concerned by a single ionization, the potential $V(\mathbf{r}_1, \mathbf{r}_2)$ is indeed short-range in the two-body scattering region $\Omega_2$(or $\Omega_1$). Therefore the kernel in the right hand side of equation (19) is compact and the results converge. The matrix elements have been calculated numerically by using the Gauss–Laguerre quadrature, that is known to be very stable, especially when deal with the orthogonal polynomials [33]. $s_{\nu\lambda}(p, Z-1)$ and $s_{nl_0}^{(n_0)}$ are the decomposition coefficients in the Sturmian basis (17) of the regular Coulomb function with the effective charge $Z-1$ and the hydrogenoid function with charge $Z$. The expression of $G_{\nu\nu',nn'}^{\lambda l((-)}(E)$ in equation (19) can be found in our previous work [35, 36]. Finally our single continuum wave function is written (7):

$$\Psi_{sc}^{(-)}(\mathbf{r}_1, \mathbf{r}_2) = \left( \frac{1 + \varepsilon \hat{P}_{12}}{\sqrt{2}} \right) \Psi_1^{(-)}(\mathbf{r}_1, \mathbf{r}_2), \tag{21}$$

with $\Psi_1^{(-)}(\mathbf{r}_1, \mathbf{r}_2)$ given by equation (19).

Let us mentioned that if in equation (19), we only keep the first term of the right-hand side and neglect the correction which involves Green's function, then we will obtain a wave function identical to that obtained by making the symmetrized product of a Coulomb function (describing the ejected electron) and a hydrogenoid function (describing the residual ion). The latter is none other than the asymptotic function of our wave function of the single continuum (21). In the section results and discussion, we will also present the curve of the TDCS obtained with this asymptotic wave function.

## 3. Results and discussion

### 3.1. Potentials and merkuriev cut-off function

In figure 1 we present the plots of the short-range $V^{(s)}$ and long-range $V^{(l)}$ potentials, for an attractive Coulomb potential. The function $V^{(s)}$ decreases rather rapidly in the three-body asymptotic domain $\Omega_0$ and coincides with the initial potential in the two-body asymptotic domain $\Omega_2$.

Figure 2 presents the plot of the Merkuriev cutt-off function $\zeta(r_2, r_1)$ with the commonly used parameters $a = 3$, $b = 20$, and $\nu = 2.1$. One realizes that the figure 2 marries well the limit given in (6), indeed in the two-body region (where $(r_2 \gg r_1)$) one sees well that $\zeta$ is very close to one (red zone) then decreases exponentially to zero (blue zone) as we approach the three-body region (where $r_1 \sim r_2 \longrightarrow \infty$).

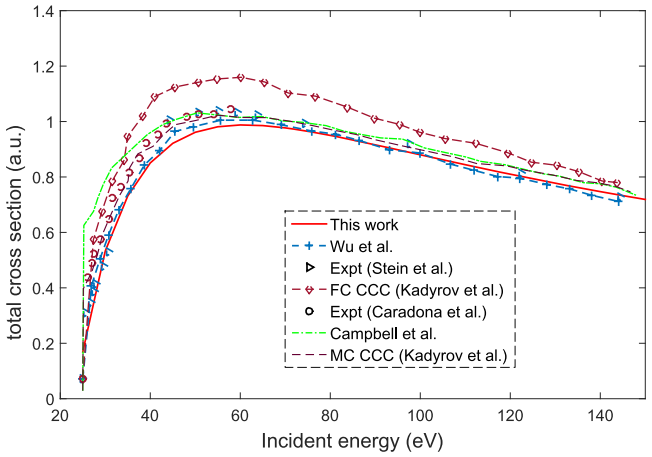


**Figure 3.** Total positron–helium cross section as a function of the energy of the incident positron above the ionization threshold. Our results given by the red solid line are compared with those obtained by other approaches: Wu *et al* [15]; Campbell *et al* [13]; FC-CCC and MC-CCC of Kadyrov *et al* [17]. Experimental data are due to Stein *et al* [12] and Caradona *et al* [37].

The theoretical approach described above to calculate the single continuum wave function is now applied to positron-impact single ionization of helium. Here, the residual ion remains in its ground state and we are limited in this work to the treatment of the channel of single ionization without taking the positronium formation and other channels into account. The result for the total positron–helium scattering cross section (widely studied) is firstly presented follow by the results of the $e^+ - \mathrm{He}$ TDCSs. Due to the lack of experimental and theoretical results for comparison in the latter case, we will cover all ejection angle values in order to predict all possible cases for the different ejection energies considered.

### 3.2. Total cross section

Figure 3 shows the total positron–helium scattering cross section as a function of the energy of the incident positron above the ionization threshold. This energy varies from the ionization threshold of helium 24.58–150 eV. The experimental results of Stein *et al* [12], Caradonna *et al* [37] as well as the theoretical results of Wu *et al* [15]; Campbell *et al* [13] and Kadyrov *et al* [17] are also shown in the figure. As it is shown in the legend, the solid red line is the result obtained within our approach. (I.e.: using the wave function in (21).) From a general point of view, all the curves have a similar shape, they have a maximum at about 55 eV and then a decrease beyond this energy. Between the energy of the ionization threshold and 55 eV, we notice a satisfactory agreement between all the theoretical approaches and the experimental results. Beyond this value, the result obtained within a frozen-core CCC approach overestimates the experimental data and the results obtained with the other theoretical methods. Utamuratov *et al* [16] explain that this overestimation is likely due to the frozen-core treatment of the He wavefunctions. Such an approximation gives a reasonably accurate ground state of He with an ionization energy of

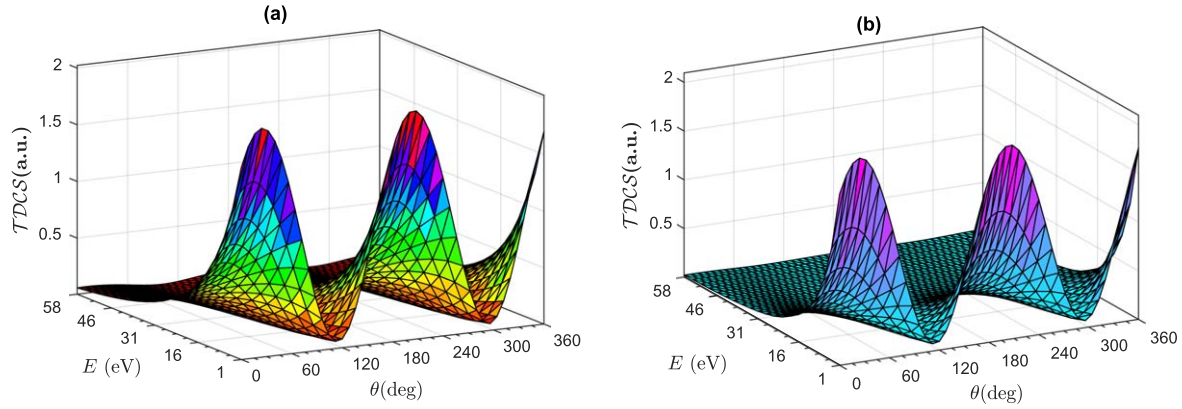


**Figure 4.** 3D representation of the TDCS of a positron-impact single ionization process of helium as a function of the energy and the angle of the ejected electron. In (a) the TDCS using the asymptotic wave function, and in (b) the TDCS using the full single continuum wave function. The positron incident energy is 700 eV.

23.74 eV instead of the actual 24.58 eV. Beyond 50 eV, the result of Campbell *et al* [13] obtained with 24 helium pseudostates and the 3 lowest Ps eigenstates, and the multi-core CCC result of Kadyrov *et al*, are very closed to our result and to the result of Wu *et al*. More other results (not presented here) of the total cross section are available in the litterature [38, 39].

### *3.3. Triple differential cross sections*

The TDCS of such process is given by:

$$\frac{\mathrm{d}^3\sigma}{\mathrm{d}\Omega_s \mathrm{d}E_s \mathrm{d}\Omega} = \frac{4p_s p}{p_0}\frac{1}{\mathrm{Q}^4}|\langle\Psi_{sc}^{(-)}(\mathbf{r}_1, \mathbf{r}_2)|2 - \exp(\mathrm{i}\mathbf{Q}\cdot\mathbf{r}_1) - \exp(\mathrm{i}\mathbf{Q}\cdot\mathbf{r}_2)|\Psi_0\rangle|^2, \quad (22)$$

where ($E_0$, $\mathbf{p_0}$), ($E_s$, $\mathbf{p_s}$), are the energy and momentum of the incident and the scattered positron. ($E$, $\mathbf{p}$), the energy and momentum of the ejected electron. $\mathbf{Q} = \mathbf{p_0}$–$\mathbf{p_s}$ is the momentum transfer.

$\Psi_0$ and $\Psi_{sc}^{(-)}$ are the initial and the final single continuum wave functions of helium. The ground state wave function $\Psi_0$ is expanded in a basis of the Coulomb Sturmian functions (17) for the radial coordinates and bipolar harmonics for the angular coordinates [32]. $\Psi_0$ is obtained as a result of diagonalization of the matrix of the Hamiltonian of the three body system. In the present calculation, we put $n_{\max} = \nu_{\max} = 20$ and $\mathrm{l}_{\max} = 3$ (maximum value for the individual angular momenta). By choosing the nonlinear parameter $\kappa_0 = 2$, we obtain $E_0 = -2.903274$ a.u. for the ground-state energy [40]. The wave function $\Psi_{sc}^{(-)}$ for the final state of the system is obtained by the method outlined above. In these calculations, it is sufficient to take into account five values (0, 1, 2, 3 and 4) of the total angular momentum $L$. The number $N$ of Coulomb sturmian functions is 50 with the dilation parameter $\kappa = 1$. The parameters of the cutoff function are the optimized one which lead to the convergence, they are $a = 3$, $b = 20$, and $\nu = 2.1$.

In order to have a global idea about the behavior of the TDCS, we first showed up its look in three-dimensional (3D) representation. Thus, we have scanned all the values that can take the angle of the ejected electron $\theta$ in the interval [0; 360] and we have also varied its energy $E$ in the interval [1; 60 eV]. For each value of $E$ within this interval, the value of the energy of the scattered positron is obtained from the law of conservation of energy.

Figure 4 shows the 3D representation of the TDCS of a positron-impact single ionization process of helium as a function of the energy and the angle of the ejected electron. The plots are done using in (a) the asymptotic wave function, and in (b) the full single continuum wave function. The positron incident energy is set at 700 eV. The both figures present a similar shape, the magnitude of cross-sections in case (a) is slightly greater than the one in case (*b*). This slightly surestimation of the cross-section in case (a) was predictable since the asymptotic wave function does not take the effects of the different correlations contained in the potential (12) into account.We observe a decrease of the values of the TDCS when the energy of the ejected electron increases. We can also observe from the both plots, two maxima located at the positions $\theta \simeq 20°$ and $\theta \simeq 200°$ and two minima located at $\theta \simeq 100°$ and $\theta \simeq 280°$. Note that the intensity observed at $\theta = 0°$ is the same at $\theta = 360°$ and should not be confused with a maximum. The two lobes structures of the plots in figure 4 can be compared and analysed in view of those observed in a process by electron impact. The first lobe with the maximum at $\theta \simeq 20°$ called binary peak, is in the direction of the momentum transfer ($+\mathbf{Q}$) and the second lobe at $\theta \simeq 200°$ called recoil peak, is in the opposite direction ($-\mathbf{Q}$).

For a better understanding of the role of these peaks in the dynamic of the collisional process, we did some two-dimensional plots of the TDCS's using the full single single continuum wave function. The plots are done for ejection energies in front, above and close to the energy of the ionization threshold of helium. The results are presented on figures.

Figure 5 gives a 2D-representation of the TDCS of a positron-impact single ionization process of helium as a function of the angle of the ejected electron and for weak ejection energies in front of the energy of the ionization

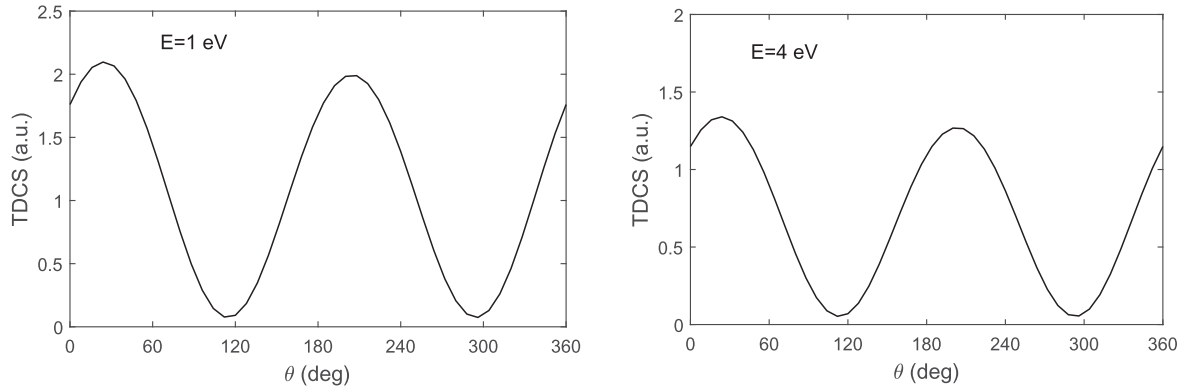


**Figure 5.** (2D) representation of the TDCS of a positron-impact single ionization process of helium as a function of the angle of the ejected electron and for weak ejection energies in front of the energy of the ionization threshold of helium. Here $E = 1$ and 4 eV.

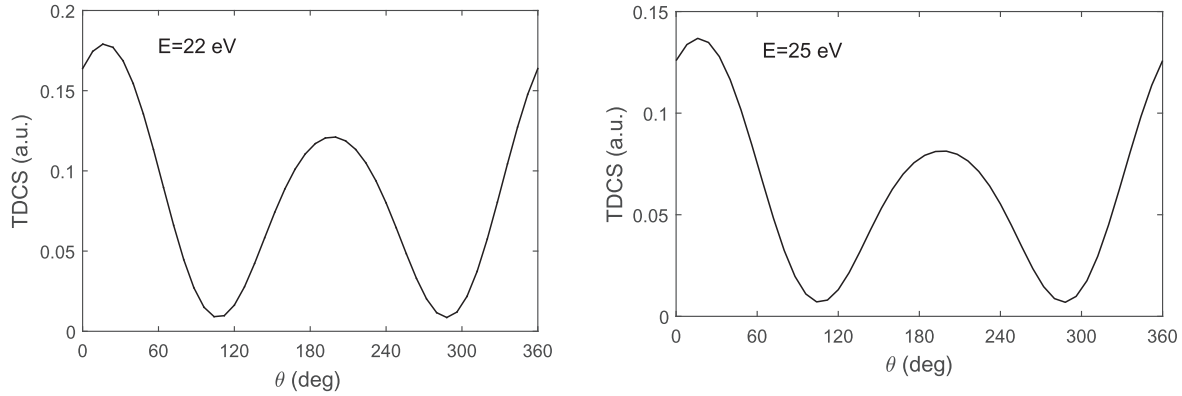


**Figure 6.** (2D) representation of the TDCS of a positron-impact single ionization process of helium as a function of the angle of the ejected electron and for ejection energies close to the energy of the ionization threshold of helium. Here $E = 22$ and 25 eV.

threshold of helium. One can easily notice that the two peaks (at 20° and 200°) have approximately the same magnitude what suggest that for weak ejection energies in front of the energy of the ionization threshold of helium, the momentum is transferred equally between the residual ion and the ejected electron. None are more involved in the collisional process than the other.

In figure 6, we have a 2D-representation of the TDCS of a positron-impact single ionization process of helium as a function of the angle of the ejected electron and for ejection energies close to the energy of the ionization threshold of helium. The first remark is the magnitude of cross-sections that is smaller compared to that observed in figure 5. Here the binary peak is dominant; which means that the momentum has been transferred in majority to the ejected electron.

Figure 7 shows a 2D-representation of the TDCS of a positron-impact single ionization process of helium as a function of the angle of the ejected electron and for large ejection energies above of the energy of the ionization threshold of helium. In this last case, one can see that the binary peak is largely dominant and therefore the momentum has been transferred almost completely to the ejected electron and the residual ion has practically remained a spectator. It can also be noted that the amplitude of the TDCS's is smaller compared to the two previous cases. Thus for a high and sufficient moderate incident positron energy (more than 10 times the energy of the ionization threshold of He), the higher the energy of the ejected electron, the lower the probability of single ionization by positron impact. Such a conclusion has also been found in [41, 42] but for elctron impact. Finally, we would like to point out that at this moderate impact-energy, non-first-Born effects are expected to start playing a role for a more better reproduction of the lobes [43, 44].

## 4. Summary

In this paper, we have use a compact-kernel-integral-equation approach built from the Faddeev–Merkuriev differential equations to calculate a three-body wave function that describes the single continuum of an atomic two-electron system. We have then applied it to positron-impact single-ionization of helium in the case where the residual ion remains in its ground state. The calculation has been performed for asymmetric coplanar geometry. The total positron–helium scattering cross section has been presented for incident-positron energies ranging from the ionization threshold to 150 eV and also the two-and three-dimensional representation of the TDCS's covering all possible values of

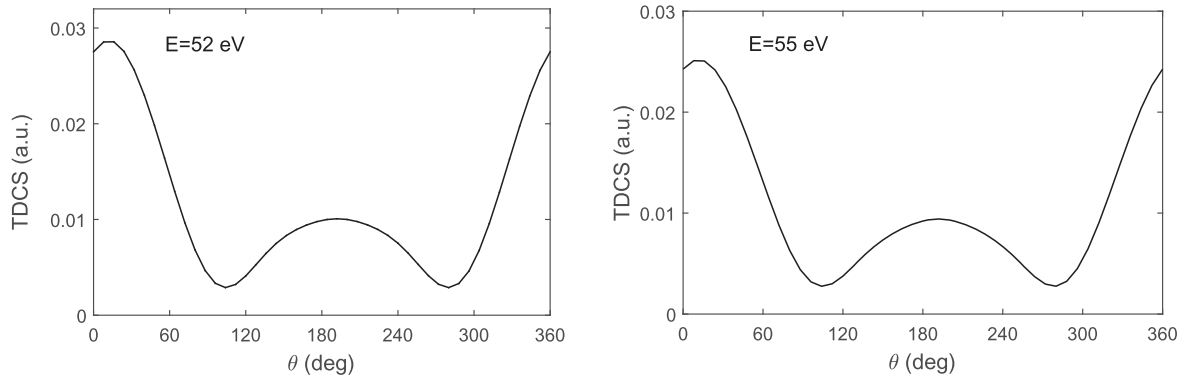


**Figure 7.** (2D) representation of the TDCS of a positron-impact single ionization process of helium as a function of the angle of the ejected electron and for large ejection energies above of the energy of the ionization threshold of helium. Here $E = 52$ and 55 eV.

the angle of the ejected electron for different values of its energy.

From the results obtained, with regard to the total cross section that we have study as a function of the energy of the incident positron, we noticed a growth in intensity between the threshold of first ionization of helium and 56 eV, then a decrease beyond this value. This is consistent with the theory in view of the agreement resulting from the comparison with the other experimental and theoretical results. With regard to the TDCS's, one can easily notice that its variations depend both on the energy of the ejected electron and on its angle. It remains important to emphasize that to our knowledge, no experimental or previous theoretical work has been done, that is why we have not been able to compare our results. From the two- and three-dimensional plots, we find that: for weak ejection energies in front of the energy of the ionization threshold of helium, the momentum is transferred almost equally between the residual ion and the ejected electron; none are more involved in the collisional process than the other. Close and above the energy of the ionization threshold, the momentum is transferred largely to the ejected electron. As regards the magnitude of TDCS, we have found that for a high and sufficient incident positron energy, the higher the energy of the ejected electron, the lower the probability of single ionization by positron impact. In other words, the positron-impact single ionization is more likely for low-energy values of the ejected electron. While waiting for new theoretical (and experimental) works on TDCs of helium at different positron-impact energies, we are of the opinion that this work could stimulate additional studies. In our current work, on the low-energy collision, that takes into account the other channels (formation of Ps, annihilation...) interfering in $e^+ - \mathrm{He}$, the continuum wave function is built with Faddeev–Merkuriev equations for three charged particles in such a way that a third term (describing the scattered positron) is added.

## Acknowledgments

The authors are grateful to the Abdus Salam International Centre for Theoretical Physics (ICTP) for its support through the OEA-AC-71 projet at the CEPAMOQ of the University of Douala-Cameroon. M S M express his gratitude to Professor B. Piraux for warm hospitality at the UCL and the active cooperation between his Laboratory and CEPAMOQ. The authors finally wish to thank Professor Gasaneo G and Professor Popov Yu V for interesting discussions about many aspects of Sturmian functions and three-body Coulomb problems.

## ORCID iDs

M Silenou Mengoue https://orcid.org/0000-0001-6192-2402

## References

[1] Bailey D L, Townsend D W, Valk P E and Maisey M N 2005 *Positron Emission Tomography* (London: Springer)
[2] Schultz P J and Lynn K G 1988 *Rev. Mod. Phys.* **60** 701
[3] Surko C M, Gribakin G F and Buckman S J 2005 *J. Phys. B: At. Mol. Opt. Phys.* **38** R57–126
[4] Massey H S W and Moussa A H 1961 *Proc. Phys. Soc.* **77** 811
[5] Parcell L A, Mc Eachran R P and Stauer A 1983 *J. Phys. B: At. Mol. Opt. Phys.* **16** 4249
[6] Campeanu R I, Fromme D, Kruse G, Mc Eachran R P, Parcell L A, Raith W, Sinapius G and Stauer A D 1987 *J. Phys. B: At. Mol. Opt. Phys* **20** 3557
[7] Knudsen H, Brun-Nielsen L, Charlton M and Poulsen M R 1990 *J. Phys. B: At. Mol. Opt. Phys.* **23** 3955
[8] Moxom J, Laricchia G and Charlton M 1993 *J. Phys. B: At. Mol. Opt. Phys.* **26** L367
[9] Humberston J W 1979 *Theoretical Aspects of Positron Collisions in Gases* (London: Academic)
[10] Van Reeth P and Humberston J W 1999 *J. Phys. B: At. Mol. Opt. Phys.* **32** 3651
[11] Mizogawa T, Nakayama Y, Kawaratani T and Tosaki M 1984 *Phys. Rev.* A **31** 2171
[12] Stein T S, Kauppila W E, Pol V, Smart J H and Jesion G 1978 *Phys. Rev.* A **17** 1600
[13] Campbell C P, McAlinden M T, Kernoghan A A and Walters H R 1998 *J. Nucl. Instrum. Meth. Phys. Res.* B **143** 41–56
[14] Igarashi A and Toshima N 1994 *Phys. Rev.* A **50** 232
[15] Wu H, Bray I, Fursa D V and Stelbovics A 2004 *J. Phys. B: At. Mol. Opt. Phys.* **37** 1165–72
[16] Utamuratov R, Kadyrov A S, Fursa D V and Bray I 2010 *J. Phys. B: At. Mol. Opt. Phys.* **43** 031001

[17] Kadyrov A S and Bray I 2016 *J. Phys. B: At. Mol. Opt. Phys.* **49** 222002
[18] Arcidiacono C, Kövér Á and Laricchia G 2005 *Phys. Rev. Lett.* **95** 223202
[19] Arcidiacono C, Beale J, Peišic Z D, Kövér Á and Laricchia G 2009 *J. Phys. B: At. Mol. Opt. Phys.* **42** 065205
[20] Kövér Á, Murtagh D J, Williams A I and Laricchia G 2010 *J. Phys. Conf. Ser.* **199** 012020
[21] Blanco F, García G, McEachran R P, Stokes P W, White R D and Brunger M J 2019 *J. Phys. Chem. Ref. Data* **48** 033103
[22] Brauner M, Briggs J S and Klar H 1989 *J. Phys. B: At. Mol. Opt. Phys.* **22** 2265
[23] Berakdar J and Klar H 1993 *J. Phys. B: At. Mol. Opt. Phys.* **26** 3891
[24] Navarette F, Della Picca R, Fiol J and Barrachina R O 2013 *J. Phys. B: At. Mol. Opt. Phys.* **46** 115203
[25] DuBois R D 2016 *J. Phys. B: At. Mol. Opt. Phys.* **49** 112002
[26] Gavin J, de Lucio O G and DuBois R D 2017 *Phys. Rev.* A **95** 062703
[27] Campeanu R I, Walters H R J and Whelan Colm T 2018 *Phys Rev.* A **97** 062702
[28] Papp Z and Plessas W 1996 *Phys. Rev.* C **54** 50
[29] Papp Z, Darai J, Hu C Y, Hlousek Z T, Kónya T and Yakovlev S L 2002 *Phys. Rev.* A **65** 032725
[30] Merkuriev S P and Faddeev L D 1993 *Quantum Scattering Theory for Several Particle Systems* (Dordrecht: Kluwer Academic)
[31] Varshalovich D A, Moskalev A N and Khersonskii V K 1988 *Quantum Theory of Angular Momentum* (Singapore: World Scientific)
[32] Foumouo E, Lagmago Kamta G, Edah G and Piraux B 2006 *Phys. Rev.* A **74** 063409
[33] Abramowitz M and Stegun I A (ed) 1966 *Handbook of Mathematical Functions, NBS Applied Mathematical Series* (Washington, DC: National Bureau of Standards)
[34] Zaytsev S A, Knyr V A, Popov Yu V and Lahmam-Bennani A 2007 *Phys. Rev.* A **75** 022718
[35] Silenou M M, Kwato N M G, Piraux B, Popov Y V and Zaytsev S A 2011 *Phys. Rev.* A **83** 052708
Silenou Mengoue M 2012 *PhD Thesis* Université de Douala
[36] Silenou Mengoue M 2013 *Phys. Rev.* A **87** 022701
[37] Caradonna P, Sullivan J P, Jones A, Makochekanwa C, Slaughter D, Mueller D W and Buckman S J 2009 *Phys. Rev.* A **80** 060701
[38] Barna I F 2004 *Eur. Phys. J.* D **30** 5–9
[39] Tökési K, Barna I F and Burgdörfer J 2005 *Nucl. Instrum. Methods Phys. Res.* B **233** 307–11
[40] Drake G W F 2006 *Handbook of Atomic, Molecular and Optical Physics* (New York: Springer)
Drake G W F and Yan Z-C 1992 *Phys. Rev.* A **46** 2378
[41] Djiokap J M N 2010 *PhD Thesis* Université Catholique de Louvain
[42] Ehrhardt H, Jung K, Knoth G and Schlemmer P 1986 *Z. Phys.* D **1** 3–32
[43] Marchalant Pascale J, Whelanz Colm T and Walters H R J 1998 *J. Phys. B: At. Mol. Opt. Phys.* **31** 1141–78
[44] Marchalant Pascale J, Rasch J, Whelanz Colm T, Madison D H and Walters H R J 1999 *J. Phys. B: At. Mol. Opt. Phys.* **32** L705–10